Aalborg Universitet

Enhanced Frequency Droop Method for Decentralized Power Sharing Control in DC Microgrids

Jafari, Mohammad; Peyghami, Saeed; Mokhtari, Hossein; Blaabjerg, Frede

Enhanced Frequency Droop Method for Decentralized Power Sharing Control in DC Microgrids

Mohammad Jafari[1], Saeed Peyghami[2], *Member, IEEE*,
Hossein Mokhtari[1], *Senior Member, IEEE,* and Frede Blaabjerg[2], *Fellow, IEEE*

Abstract— **This paper proposes two novel approaches to improve the superimposed frequency droop scheme for the control of DC microgrids. Conventional voltage-based control strategies suffer from issues such as undesirable voltage regulations, poor power sharing among the sources, and negative effects of line resistances on the equivalent droop characteristics. To overcome these challenges, a superimposed frequency droop scheme has been introduced. However, this method suffers from three major issues which are (i) instability in terms of load variation which is due to the location of system dominant poles, (ii) limitation in system loading due to the limitation in the transferred reactive power, and (iii) poor voltage quality caused by the injection of the AC voltage. In this paper, two methods are presented to stabilize the system and enhance its loading condition, consequently improving its viability for control of DC microgrid. Furthermore, system voltage quality is improved by limiting the amplitude of the injected AC voltage. The effectiveness of the proposed schemes is shown by different simulations and further validated by experiments.**

Index Terms—**Microgrids, DC Microgrids, Superimposed Frequency Droop Scheme, Injected AC Voltage, System Stability, System Loading, Voltage Quality.**

I. INTRODUCTION

Global paradigm shift towards decarbonization and economization of energy sector has intensified the necessity of electric power system modernization. Distributed generations (DGs) in low/medium voltage grids have revolutionized the structure of conventional power systems from centralized, top-down paradigm to distributed, bottom-up manner. Meanwhile, proliferation of DGs introduces more functionalities to distribution systems in both grid-connected and islanded modes. Moreover, microgrid (MG) and smart grid technologies are facilitating the smarter operation of DGs in a liberalized environment. Hence, the future power systems will be made up of clusters of AC-DC MGs [1] as shown in Fig. 1.

Reliable and optimal operation and control of such systems require strong communication infrastructure to share power and energy information among the DGs and operators [2]. Hierarchically, MGs can be controlled by three levels of primary, secondary and tertiary controllers [3]. The primary control is in charge of local power sharing for preventing overstressing the units and voltage/frequency forming by the DGs. The secondary control is responsible for the voltage/frequency regulation/restoration in MGs. The tertiary control is associated with optimal and economical operation of DGs and MGs. A communication system is required to make coordination among DGs and MGs for optimal and reliable operation.

Employing communication among all units in clusters of MGs in three levels of power and energy management hierarchy can make the system vulnerable. It introduces control complexity, high infrastructure investment and low security in terms of cyber-attacks. Hence, decentralized approaches are preferred in, at least, the primary and secondary levels of the control strategy to eliminate the communication systems consequently introducing low investment costs and high security. Hence, this paper aims at proposing a decentralized control approach in DC MGs as a segment of future distribution systems.

Conventionally, DC systems are controlled using voltage-based droop control strategies. In these methods, the changes of each unit voltage work as a signal indicating the power balance among the sources and loads. These methods are known with the name of DC bus signaling (DBS) [4]-[7]. However, DBS methods suffer from some major issues. Unlike frequency in AC systems, the voltage is a local parameter. Therefore, using the voltage as a base signal to control the system leads to some levels of inaccuracy. Besides, transmission line resistances change the equivalent current-voltage droop characteristics. This causes poor current-sharing among the sources in a MG, where some sources might become overloaded. High droop gains alleviate the effects of transmission line resistances. But, voltage regulation of the system deteriorates due to severe voltage drops on the droop gains [3]. To enhance the system voltage regulation, another level of controller called the secondary controller is added to the system [8]-[11]. But, the communication infrastructure used in the secondary controller affects the overall reliability of the system [12], [13]. In order to alleviate load sharing errors and voltage drops, adaptive PI controllers are adopted for regulating droop gains and enhancing the performance of secondary controllers in [14]. In [15], droop gains are adapted regarding the estimated line resistances in order to alleviate the negative impact of line resistances. However, both of these methods increase system complexity and require further communication infrastructure that affect the system reliability and stability. To increase power sharing accuracy, a nonlinear droop strategy is presented in [16]. However, this method increases system complexity and nonlinearity for large systems. The adaptive droop schemes presented in [17]-[19] enhance power sharing accuracy of the

[1]Mohammad Jafari and Hossein Mokhtari are with the Center of Excellence in Power System Management and Control, Department of Electrical Engineering, Sharif University of Technology, Tehran, Iran (e-mail: m.jfr.m74@gmail.com and mokhtari@sharif.edu).

[2]Saeed Peyghami and Frede Blaabjerg are with the Department of Energy Technology, Aalborg University, Aalborg, Denmark (email: sap@et.aau.dk and fbl@et.aau.dk).
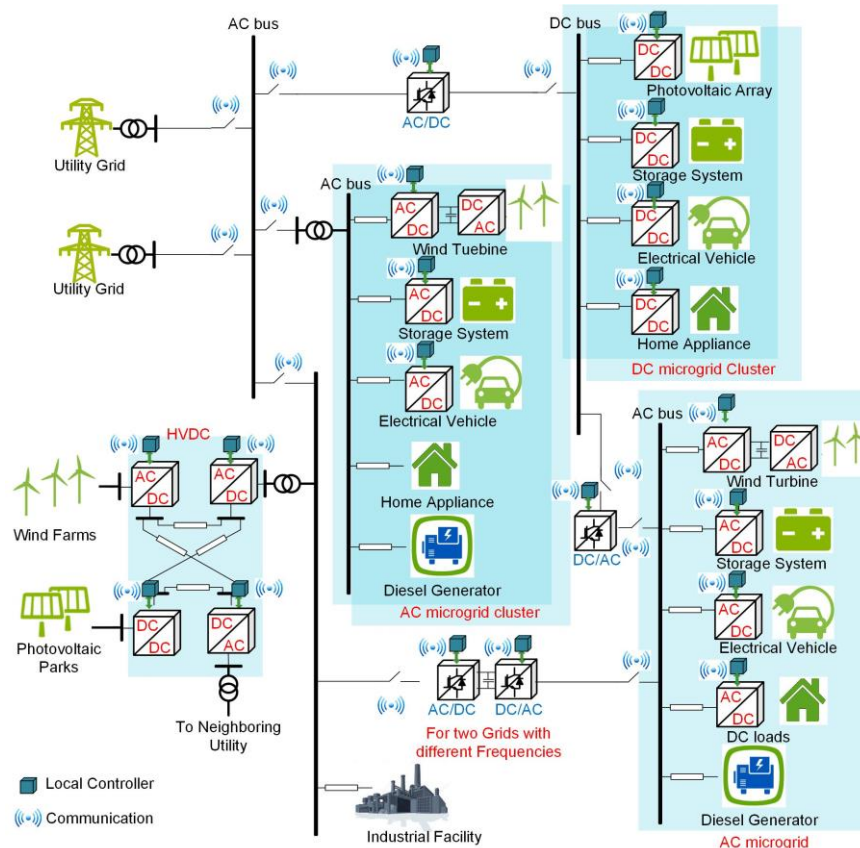
Fig. 1. A general structure of future power systems.

system. However, these schemes are sensitive to line resistances. In [20] and [21], a new control strategy using the square of the voltage-power droop characteristic is proposed to alleviate power-sharing mismatches and ensure system stability at the presence of constant power loads(CPL). Moreover, a control strategy with an adaptive droop characteristic is introduced in [22]. To compensate the voltage drops and negative effects of line resistances, voltage reference and droop gains are changed according to the system load level. However, it must be noticed that all the aforementioned methods suffer from some levels of inaccuracy in load sharing and voltage regulation. A master-slave based decentralized approach has been introduced in [23], where the master unit modulates its terminal voltage as an AC ripple superimposed on the DC voltage. While this approach eliminates the communication systems in DC MGs, its viability in terms of loss of master unit has not been demonstrated.

To overcome the aforementioned issues, a decentralized frequency droop control strategy based on a superimposed AC voltage is presented in [24]. The superimposed frequency droop method (SFDM) is originally adopted from AC frequency droop in conventional power systems, where the global frequency of the system is used to share the loads power among the plants. Therefore, unlike the voltage which is a local parameter, using the frequency of the superimposed AC voltage results in an acceptable control of the MGs. The frequency droop scheme can appropriately perform the load-sharing and voltage regulation in a DC MG without utilizing any physical communication system. However, the performance of system at

high/low load levels is limited due to the stability issues. This has been addressed in [25] where the frequency droop is merged with the conventional droop control. In this approach, a decentralized secondary scheme is also employed to compensate the MG voltage drops due to the conventional droop gains. This introduces control system difficulty in the case of large DC MGs with several DGs. Thus, this paper proposes two adaptive schemes in order to improve the performance of the frequency droop scheme presented in [24] for a wide range of load variations without any stability issues and control complexity. In this paper, an adaptive voltage coupling gain (AVCG) and an adaptive amplitude of the injected AC voltage (AAIV) schemes are proposed to stabilize the SFDM and enhance its loading condition. In the proposed AVCG scheme, the voltage coupling gains are changed according to the system overall load level to ensure the system stability. In the proposed AAIV scheme, the amplitude of the injected AC voltage is adjusted according to the system loading to improve the system load sharing. Using the proposed methods, much wider range of loads can be supplied by the system. Furthermore, the proposed methods do not affect the system voltage regulation and load-sharing accuracy.

This paper is structured as follows. In section II, a brief introduction of the SFDM is provided. This is followed by an analysis on the effects of voltage coupling gains and the amplitude of the injected AC voltage on the transferred reactive power in section III. The proposed methods and their small signal stability analysis are given in sections IV, and V, respectively. Simulation results are provided in section VI,
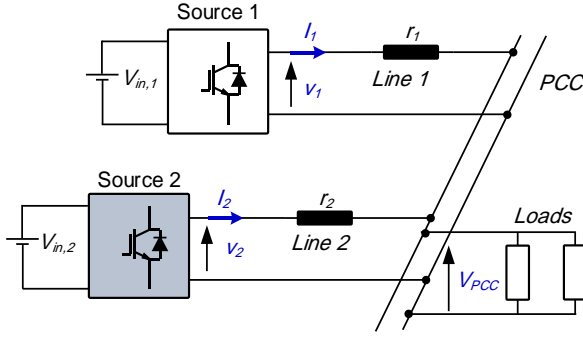
Fig. 2. Single line diagram of a DC microgrid with two DGs and localized loads ($V_{DC,ref} = 700$ V, $r_1 = 2$ Ω, $r_2 = 4$ Ω).
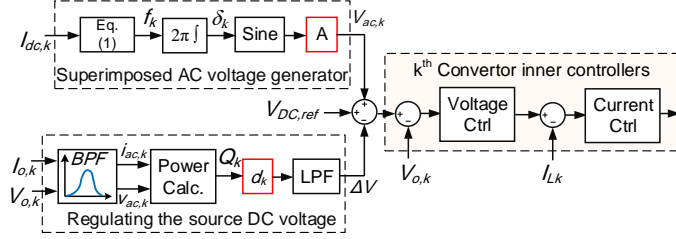

Fig. 3. Control block diagram of the SFDM [24] (I_{ok} and V_{ok} are the kth convertor output current and output voltage).
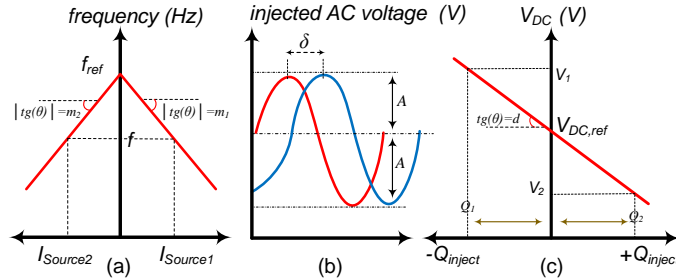

Fig. 4. Schematic of (a) frequency droop characteristic (b) injected AC voltage (c) regulation of DC voltages in terms of the injected reactive power [25]

which is followed by the experimental results in section VII. Finally, section VIII concludes the paper.

II. THE SUPERIMPOSED FREQUENCY DROOP METHOD (SFDM)

The main idea of the SFDM is adopted from AC systems, where the system global frequency is used for the power sharing among the plants. In this method, a small AC voltage is injected to the main DC system, where the frequency of this injected AC voltage is proportional to the output DC current of the corresponding source. The power balance among the sources is ensured using a frequency droop characteristic [24]. At steady state operation of the system, all the sources are synchronized, and the frequency of the superimposed AC voltage of the sources is calculated as:

$$f = f_{ref} - m_k I_k, \quad k = 1, ... , N \qquad (1)$$

where f is the system frequency, f_{ref} is the system reference frequency, N is the number of sources, and I_k and m_k are the output DC current and frequency droop gain of the kth source.

In SFDM, the transferred reactive power works as a coupling power among the sources, and is used to regulate the DC voltage of the sources [24]. Source voltages are calculated as
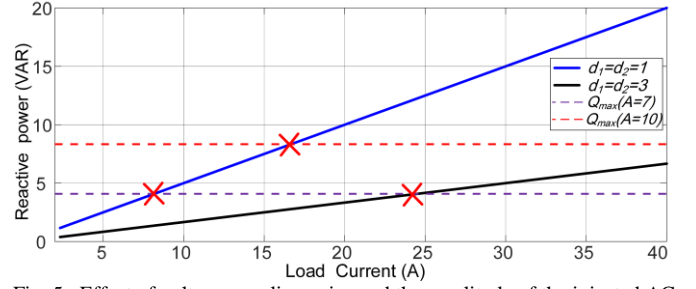

Fig. 5. Effect of voltage coupling gains and the amplitude of the injected AC voltage on the system maximum loading ($15 < R_{load} < 250$ Ω, $m_1 = m_2 = 0.15$)
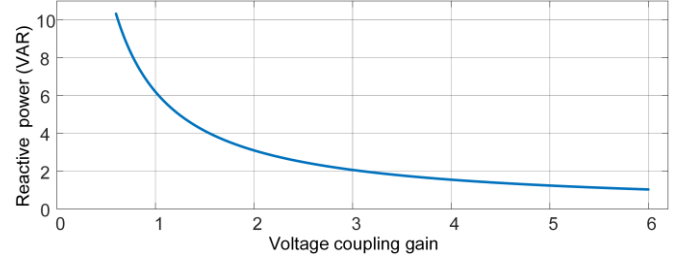

Fig. 6. Effect of voltage coupling gains on the transferred reactive power at a constant load ($R_{load} = 55$ Ω, $m_1 = m_2 = 0.15$).

(2) in the SFDM. Fig. 2 shows a typical DC MG with two sources and local loads. The control block diagram of the SFDM is depicted in Fig. 3, where the superimposed AC voltage $V_{ac,k}$ with a constant amplitude of A is given to the input of the convertor controllers.

$$V_k = V_{DC,ref} - d_k Q_k, \quad k = 1, ... , N \qquad (2)$$

where $V_{DC,ref}$ is the MG reference voltage and V_k is the voltage of the kth source. Q_k and d_k are the injected reactive power and the voltage coupling gain of the kth convertor.

The applied LPF in Fig. 3 is for damping and filtering out power oscillations and does not have any impact on the steady state operation of the system [25]. The schematic of the applied frequency droop characteristic is depicted in Fig. 4(a). As shown in this figure, the frequency of the injected AC voltage is proportional to the current of the corresponding source and will decrease as the load increases. The DC voltage of a typical source and its variation in terms of the injected reactive power is depicted in Fig. 4(c). As shown in this figure, DC voltage of the buses are regulated using the transferred reactive power [25]. In other words, the transferred reactive power changes the DC voltages in such a way to synchronize the frequency of the injected AC voltage of all the sources. As shown in Fig. 3 and Fig. 4(c), the transferred reactive power affects the DC voltage of the sources. The DC voltage of the sources have a direct impact on DC current of the loads and, therefore according to (1), they will affect the frequency of the injected AC voltage. As shown in Fig. 3 and Fig. 4(b), the frequency of the injected AC voltage has a direct impact on the angle of the injected AC voltage i.e. δ. The angle of the injected AC voltage directly affects the transferred reactive power, which will be further discussed in section III. This loop shows how the transferred reactive power, the DC voltage of the sources, and the frequency of the injected AC voltage change in order to achieve an accurate control of the system [25].

III. TRANSFERRED REACTIVE POWER AND THE EFFECTIVE PARAMETERS

For simplicity, the test system in Fig. 2 with two DGs is considered. According to [24] and noting that the load does not consume any reactive power, the required transferred reactive power among the two sources at steady state operation of the system is calculated as:

$$Q = Q_1 = \frac{V_{DC,ref}(m_1 r_2 - m_2 r_1)}{R_{load}(d_1 + d_2)(m_1 + m_2) + r_1 d_2 m_2 + r_2 d_1 m_1}. \quad (3)$$

where r_1 and r_2 are the transmission line resistances and R_{load} is the load resistance.

For the system in Fig. 2, the voltage of the buses and the load current can be calculated as:

$$\begin{cases} V_k = V_{PCC} + r_k I_k \ , \quad k = 1,2; \\ V_{PCC} = R_{Load} I_{Load} \end{cases} \quad (4)$$

$$I_{load} = I_1 + I_2 . \quad (5)$$

By putting the value of Q from (3) into (2), the value of the sources voltages can be calculated. Therefore, using the calculated bus voltages, (4) and (5), the value of I_{Load} is calculated as (6).

$$I_{Load} = \frac{V_{DC,ref}(d_1 + d_2)(m_1 + m_2)}{R_{Load}(d_1 + d_2)(m_1 + m_2) + r_1 d_2 m_2 + r_2 d_1 m_1} \quad (6)$$

By finding R_{Load} according to I_{Load} from (6) and placing it into (3), the value of the transferred reactive power in terms of the load current is calculated as (7).

$$Q = I_{Load} \times \frac{m_1 r_2 - m_2 r_1}{(d_1 + d_2)(m_1 + m_2)} \quad (7)$$

Using (7) for the system in Fig. 2, variations of the transferred reactive power in terms of load variations is depicted in Fig. 5. As shown in this figure, the transferred reactive power increases as the system load increases. However, with a constant amplitude of the injected AC voltage, the maximum transferrable reactive power is limited. The injected reactive power of the two sources, and the maximum transferrable reactive power at the steady state operation of the system are calculated as [24]:

$$\begin{cases} Q_1 = \frac{A^2}{2(r_1 + r_2)} \sin\delta \\ Q_2 = -\frac{A^2}{2(r_1 + r_2)} \sin\delta \end{cases} \quad (8)$$

$$Q_{max} = \frac{A^2}{2(r_1 + r_2)} \quad (9)$$

where $\delta = \delta_1 - \delta_2$, and δ_1 and δ_2 are the angle of the injected AC voltage of the sources one and two.

As shown in Fig. 5, the maximum loading of the system depends on both the voltage coupling gains and the amplitude of the injected AC voltage. The higher the amplitude of the injected AC voltage, the higher the maximum loading of the system. This is also true for the voltage coupling gains. Variations of the transferred reactive power in terms of the variation of the voltage coupling gains at a constant load is shown in Fig. 6.

With a constant value of the injected AC voltage amplitude and the voltage coupling gains, the maximum loading of the
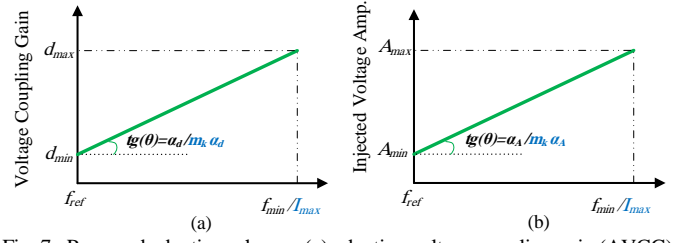

Fig. 7. Proposed adaptive schemes (a) adaptive voltage coupling gain (AVCG) (b) adaptive amplitude of the injected AC voltage (AAIV).
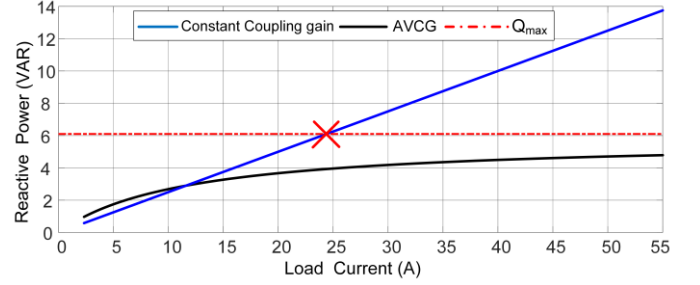

Fig. 8. The transferred reactive power in the proposed AVCG (A = 8.5 V, d_{min} = 1, α_d = 1.15, constant droop gains = 2, $m_1 = m_2 = 0.15$)

system is limited. High values of the voltage coupling gains and the injected AC voltage amplitude enhance the system loading condition. However, the system stability is another concern at low loads. This is due to the location of the system dominant poles. In these cases, the imaginary parts of the system poles are high, and the system damping ratio is low. This leads to system instability at low loads. This matter is further explained and simulated in section V and VI. Moreover, high amplitude of the injected AC voltage deteriorates the voltage quality of the system. Then, the system stability, loading condition and voltage quality are the main challenges in choosing the voltage coupling gains and the amplitude of the injected AC voltage. In fact, it is not possible to accomplish all these challenges with constant values of the voltage coupling gains and the injected AC voltage amplitude.

IV. PROPOSED ADAPTIVE CONTROL METHODS

As mentioned in section III, it is only possible to supply a limited range of system loading with a constant value of the injected AC voltage and the voltage coupling gains. Therefore, an adaptive voltage coupling gain and an adaptive amplitude of the injected AC voltage can be applied to solve the stability issue and enhance the system loading condition. The two methods presented have the same effect on system overall stability, and they can be used to ensure system stability at different loadings.

A. Adaptive Voltage Coupling Gain (AVCG)

As shown in Fig. 6, voltage coupling gains have a major effect on the transferred reactive power. High voltage coupling gains decrease the transferred reactive power at a constant load, and the transferred reactive power reaches its maximum at higher loads. Therefore, higher loads can be supplied with high coupling gains. However, the system stability is affected at low loads due to the low damping ratio of the system. This is further explained in section V. Therefore, high droop gains at high

loads, and low droop gains at low loads are required for stable operation of the MG. This is the basic concept of the proposed AVCG scheme. In the proposed scheme, the coupling gains are adjusted regarding the system overall load level.

The coupling gains must be set according to the system loading level. Therefore, a criterion is required to determine the overall loading of the system. The system frequency is one of the best choices for this purpose. In the SFDM, the system frequency drops as the load increases, and therefore, it is proportional to the overall loading level of the MG. Besides, it is a global parameter, and is available in the whole MG. The proposed AVCG scheme for the SFDM is presented in Fig. 7(a). The sources voltage coupling gains are determined as:

$$d_i = d_{min} + \alpha_d (f_{ref} - f) \quad (10)$$

where α_d is the change ratio of the voltage coupling gains according to the system frequency, d_{min} is the voltage coupling gain at no-load condition, and d_i is the voltage coupling gain of the ith source.

The accepted trend in controlling DC grids for voltage regulation is to regulate the average voltage of the voltage-controlled buses and to make sure that it is equal to the system reference voltage. Therefore, due to the voltage regulation considerations, d_{min} and α_d of all the sources must be equal. This leads to the equality of all the sources voltage coupling gains at steady state operation of the system. Hence, using the proposed AVCG scheme, the average voltage of the voltage controlled buses is equal to the system reference voltage. With refer to [24], the average voltage of the voltage controlled buses at the steady state operation of the system is as:

$$V_{average} = \frac{1}{N}\sum_{k=1}^{N}V_k = \frac{1}{N}\sum_{k=1}^{N}(V_{DC,ref} - d_k Q_k) = V_{DC,ref} - \frac{d}{N}\sum Q_k = V_{DC,ref}.$$
$$(11)$$

At the steady state operation of the MG, the sources output currents are related as [24]:

$$\frac{I_1}{I_2} = \frac{m_2}{m_1} . \quad (12)$$

Therefore, the output DC currents of the sources can also be used for determining the voltage coupling gains. substituting (1) into (10) yields:

$$d_i = d_{min} + \alpha_d m_i I_i . \quad (13)$$

$$\alpha_d = \frac{d_{max} - d_{min}}{f_{ref} - f_{min}} = \frac{d_{max} - d_{min}}{m_i I_{i,max}}. \quad (14)$$

α_d is calculated as (14), where f_{min} and d_{max} are the system frequency and the sources voltage coupling gains at the system maximum loading. $I_{i,max}$ is the rated current of the ith source. It must be noted that d_{max} / d_{min} must be chosen in such a way that

the system has an acceptable and stable performance at the maximum /minimum loading of the system.

For the system in Fig. 2, the transferred reactive power with a constant coupling gain and the proposed AVCG scheme is depicted in Fig. 8. Having used the proposed AVCG scheme, the transferred reactive power stays within an acceptable range. Therefore, it is possible to supply higher loads with lower amplitude of the injected AC voltage. Hence, the voltage quality of the system is also enhanced.

The control block diagram of the proposed AVCG scheme is shown in Fig. 9(a). As shown in this figure, the frequency of the injected AC voltage is determined by its corresponding frequency droop characteristic, and the DC voltage of the source is regulated using the transferred reactive power and the proposed AVCG.

B. Adaptive Amplitude of the Injected AC Voltage (AAIV)

As mentioned, with a constant value of the injected AC voltage and the voltage coupling gains, it is only possible to supply a limited range of loads. Using a high amplitude of the injected AC voltage, higher loads can be supplied by the MG. However, system instability at low loads and poor voltage quality are the main concerns in this case. With low amplitude of the injected AC voltage, the system voltage quality and stability are desirable at low loads. However, due to limitation in the transferred reactive power, the system maximum loading is limited.

In the proposed AAIV scheme, the amplitude of the injected AC voltage is determined according to the system load level. In the SFDM, the system frequency and the DC current of each source can be used to determine the overall load of the MG. For AAIV, variation of the amplitude of the injected AC voltage in terms of the system load is depicted in Fig. 7(b), and the amplitude of the injected AC voltage is determined as:

$$A = A_{min} + \alpha_A (f_{ref} - f) \quad (15)$$

$$A = A_{min} + \alpha_A m_i I_i \quad (16)$$

$$\alpha_A = \frac{A_{max} - A_{min}}{f_{ref} - f_{min}} = \frac{A_{max} - A_{min}}{m_i I_{i,max}} \quad (17)$$

where A_{max} and A_{min} are the amplitude of the injected AC voltage at full-load and no-load conditions. α_A is the change ratio of the injected AC voltage amplitude according to the system frequency. It is crucial to design A_{max} / A_{min} such that the system has a stable performance at the maximum /minimum loading of the system.

Using the proposed AAIV, the system stability is ensured and its loading condition is enhanced. Besides, the amplitude of the injected AC voltage is restricted at low load levels. Therefore,
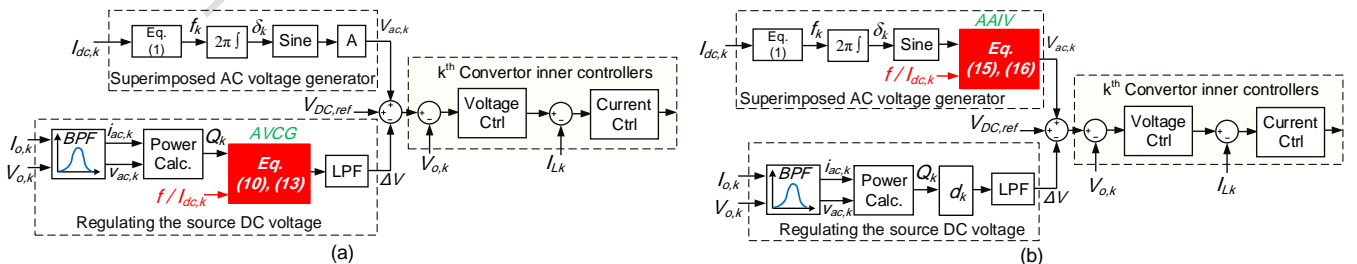

Fig. 9. Control block diagram of the proposed adaptive schemes for the kth source (a) adaptive voltage coupling gain (AVCG) (b) adaptive amplitude of the injected voltage (AAIV).
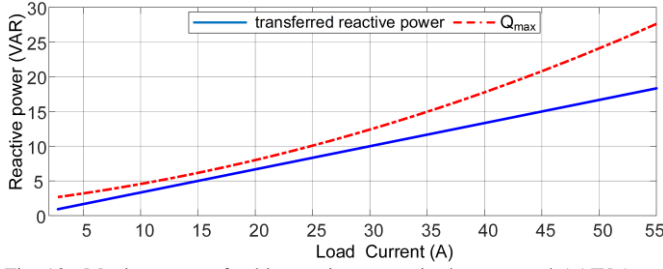
Fig. 10. Maximum transferable reactive power in the proposed AAIV ($m_1 = m_2 = 0.15$, $A_{min} = 5$V, $\alpha_A = 3.2$, $d = 1.5$).

the voltage quality of the system is improved at low loads. For the system in Fig. 2, variations of the maximum transferred reactive power in terms of the system load current is depicted in Fig. 10. As this figure shows, the maximum transferrable reactive power is regulated according to the system loading, and the transferred reactive power is always below the limited value. The control block diagram of the proposed AAIV scheme is depicted in Fig. 9(b). As shown in this figure, the frequency and amplitude of the injected AC voltage is determined by the output DC current of the corresponding source.

V. SMALL SIGNAL STABILITY ANALYSIS

In this section, the stability of the proposed schemes is analyzed using the small signal stability analysis. According to [25], in the SFDM, the converter and its inner controllers are designed in such a way to have much higher bandwidth as compared to the frequency of the injected AC voltage. Therefore, due to the fast dynamics of the inner voltage and current controllers, the performance of the system associated with the power-sharing loop is only investigated.

A. AVCG scheme

At the steady state operation of the system in Fig. 2, source voltages, the PCC voltage, and δ are as [24]:

$$V_k = V_{PCC} + r_k I_k \tag{18}$$

$$V_{PCC} = R_{load}(I_1 + I_2) \tag{19}$$

$$\delta = \frac{2\pi}{S}(m_2 I_2 - m_1 I_1) \tag{20}$$

where V_{PCC} is the voltage of PCC, and S is the Laplace operator. Substituting (13) into the linear form of (2) yields:

$$\begin{cases} \Delta V_1 = -d_{10}G_{(s)}\Delta Q_1 - Q_{10}G_{(s)}\Delta d_1 \\ \Delta V_2 = -d_{20}G_{(s)}\Delta Q_2 - Q_{20}G_{(s)}\Delta d_2 \end{cases} \tag{21}$$

where d_{10} and d_{20} are the voltage coupling gains, and Q_{10} and Q_{20} are the injected reactive power of the sources one and two, respectively. $G(s)$ is the low-pass filter with the cutoff frequency of w_c ($G(s) = w_c/(S+w_c)$).

Substituting (21) and the linear model of (8) into the linear models of (18) and (19), the linear models of I_1 and I_2 are calculated. Substituting ΔI_1 and ΔI_2 into the linear model of (20), the characteristic equation of the system using AVCG is found as:

$$S^2 + w_c S + \frac{\beta_1}{g_1} = 0 \tag{22}$$

where β_1 and g_1 are calculated as:
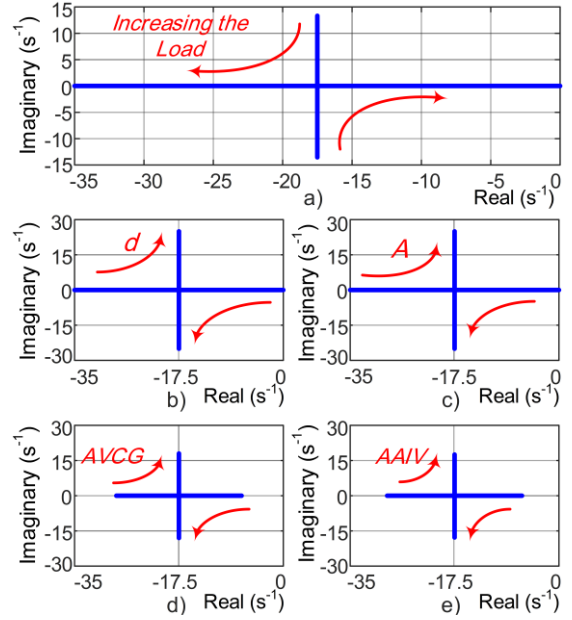

Fig. 11. Variation of the system dominant poles location ($m_1 = m_2 = 0.15$) (a) effect of increasing the load in SFDM ($15.3 < R_{load} < 100$ Ω) (b) effect of increasing the voltage coupling gains in the SFDM ($0.6 < d < 6$) (c) effect of increasing the amplitude of the injected AC voltage in SFDM ($5.4 < A < 15$V) (d) effect of increasing the load in the proposed AVCG ($15 < R_{load} < 250$ Ω) (e) effect of increasing the load in the proposed AAIV ($15 < R_{load} < 250$ Ω).

$$g_1 = r_1 r_2 + R_{load}(r_1 + r_2) \tag{23}$$

$$\beta_1 = 2\pi\omega_c k_\delta R_{load}\left[\begin{array}{l} d_{10}\left(m_2 + m_1\dfrac{(r_2 + R_{load} - Q_{10}\alpha m_2)}{R_{load}}\right) \\ +d_{20}\left(m_1 + m_2\dfrac{(r_1 + R_{load} + Q_{10}\alpha m_1)}{R_{load}}\right) \end{array}\right] \tag{24}$$

where k_δ in (20) is calculated by linearizing (2) as:

$$k_\delta = \frac{A^2}{2(r_1 + r_2)}\cos\delta_0 . \tag{25}$$

Using the SFDM for the system in Fig. 2, and with $d_1 = d_2 = 2.5$ and $A = 10$V, variations of the system poles in terms of load variation is depicted in Fig. 11(a). With constant coupling gains and constant amplitude of the injected AC voltage, the variation of the system poles location in terms of load variation is very high. Therefore, the system stability is the main concern in the SFDM. As shown in Fig. 11(a), the imaginary parts of the system poles are very large at low loads, and the system damping ratio is low. This results in an unstable operation of the system at low loads. At high loads, the system poles move toward the imaginary axis, which results in system instability.

The effect of the voltage coupling gains on the location of the system poles at constant load and $A = 10$V is depicted in Fig. 11(b). As shown in this figure, increasing the voltage coupling gains alleviates the effect of increasing the load on the system poles location. Using (18) for the proposed AVCG, and with $A = 8$V, $d_{min} = 1.3$, and $\alpha_d = 1.65$, the location of the system poles at different load levels is depicted in Fig. 11(d). Using the proposed AVCG, the system damping ratio is high at low loads. As the load increases, the system poles move away from the imaginary axis. Therefore, the proposed ADVG guarantees the stable operation of the MG at all load levels, and a much wider range of the loads can be supplied by the system.

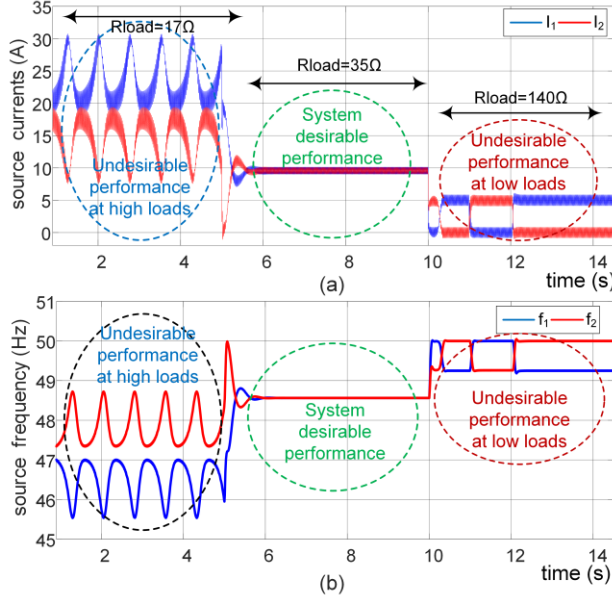| Symbol	Definition	Value
V_{in}, V_{out}	Input, Output voltage	540 V, 700 V
L_{dc}, C_{dc}	DC inductor, capacitor	2 mH, 500 µF
f_{sw}	Switching frequency	20 kHz
$k_{pv}+k_{iv}/S$	Voltage controller	1.5 + 20/S
$k_{pi}+k_{ii}/S$	Current controller	0.05 + 1/S

Fig. 12. Simulation results for the SFDM ($m_1 = m_2 = 0.15$, $A = 8$ V, $d_1 = d_2 = 5$) (a) source currents (b) frequency of the injected AC voltage of the sources.

B. AAIV scheme

For the system in Fig. 2, substituting the linear model of (16) into (8) yields:

$$\begin{cases} \Delta Q_1 = -k_1 m_1 \Delta I_1 - k_2 \Delta \delta \\ \Delta Q_2 = k_2 m_2 \Delta I_2 + k_2 \Delta \delta \end{cases} \quad (26)$$

where k_1 and k_2 are calculated as:

$$\begin{cases} k_1 = \dfrac{A_0 \alpha_A}{r_1 + r_2} \sin \delta_0 \\ k_2 = \dfrac{A_0^2}{2(r_1 + r_2)} \cos \delta_0 . \end{cases} \quad (27)$$

Using (26) and the linear models of (2), (18)- (20), the characteristic equation of the system using AAIV is calculated as:

$$s^2 + w_c s + \frac{\beta_2}{g_2} = 0 \quad (28)$$

where β_2 and g_2 are calculated as:

$$g_2 = r_1 r_2 + R_{load} (r_1 + r_2) + k_1 d_2 m_2 (R_{load} + r_1) \\ - k_1 d_1 m_1 (R_{load} + r_2) - k_1^2 d_1 d_2 m_1 m_2 \quad (29)$$

$$\beta_2 = 2\pi R_{load} k_2 \omega_c \left[\begin{array}{l} m_1 \left(d_1 \times \dfrac{(R_{load} + r_2 + k_1 d_2 m_2)}{R_{load}} + d_2 \right) \\ + m_2 \left(d_1 + d_2 \times \dfrac{(R_{load} + r_1 - k_1 d_1 m_1)}{R_{load}} \right) \end{array} \right]. \quad (30)$$

At constant load and $d_1 = d_2 = 2.5$, the effect of increasing the amplitude of the injected AC voltage on the location of the

system poles is depicted in Fig. 11(c). As shown in this figure, increasing the amplitude of the injected AC voltage mitigates the effect of the load increase. For the MG using the proposed AAIV, and parameters of $d_1 = d_2 = 5$, $A_{min} = 4V$, and $\alpha_A = 1.7V/Hz$ the root locus is depicted in Fig. 11(e). At low loads, the imaginary part of the system poles is very low which yields a high damping ratio, and a desirable operation of the system at low loads. At high loads, the system poles move away from the imaginary axis. Having used the proposed AAIV, the poles of the system are located within an acceptable area, and a much wider range of the loads can be supplied by the MG.

Comparing the root locus of the two proposed strategies in Fig. 11(d) and Fig. 11(e) shows that the two methods proposed in the paper have almost similar effects on the overall performance of the system and both can be used to solve the instability problem of the SFDM.

VI. SIMULATION RESULTS

In this section, three simulation cases are provided to study the performance of the proposed adaptive control strategies. In case I, the instability of the system using the SFDM is investigated at low and high loads. The performance of the proposed AVCG and AAIV schemes are simulated in the cases II and III, respectively. The simulated system is shown in the Fig. 2, which includes two boost convertors as the power sources that are connected to PCC. The boost convertor parameters and its inner controllers are given in Table I.

A. Case I: SFDM

In this case, the performance of the SFDM is investigated through the simulations and the results are shown in Fig. 12. As mentioned earlier, with the SFDM, only can a limited range of the loads be supplied by the system. This is shown in Fig. 12, where the system reaches instability at high loads due to the limitation in the transferred reactive power. The system performance is acceptable at $I_{load} = 20$ A. However, as shown in Fig. 12, the system performance is not desirable at low loads due to the low damping ratio. Increasing/decreasing the voltage coupling gains or the amplitude of the injected AC voltage enhances the system performance at high/low loads. However, this will deteriorate the system performance at wide range of load variation.

B. Case II: proposed AVCG scheme

In this case, the performance of the proposed AVCG is simulated at different load levels, and the simulation results are depicted in Fig. 13. The load current varies from high levels down to the low levels, and the system works perfectly at all load levels. The system frequency profile is depicted in Fig. 13(b). In fact, the stability of the system frequency attests the perfect performance of the system at all load levels using the proposed AVCG scheme. The source voltages and the average voltage of the voltage-controlled buses are depicted in Fig. 13(c). As shown in this figure, the system presents a perfect voltage regulation, and the average voltage of the voltage-controlled buses is equal to the MG reference voltage. The injected reactive power profile of the two sources is depicted in
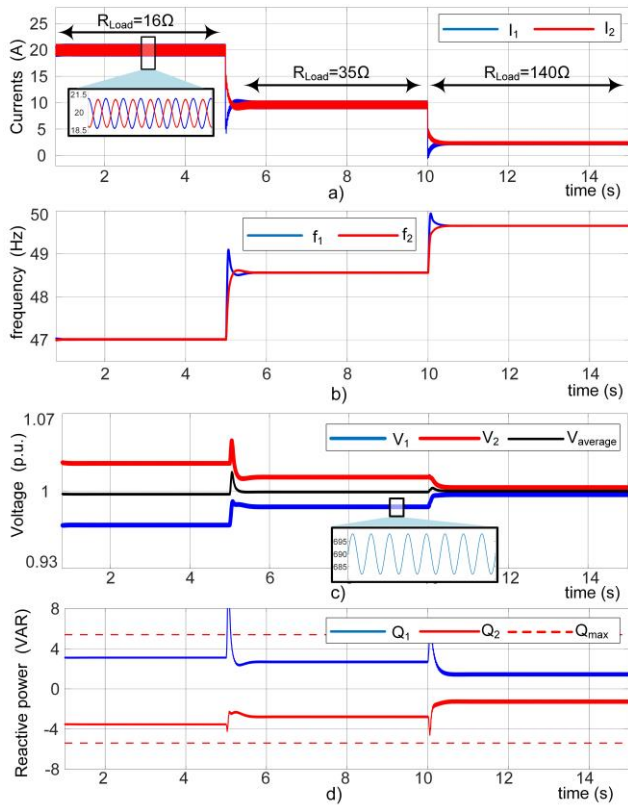
Fig. 13. Simulation results for the proposed AVCG ($m_1 = m_2 = 0.15$, $A = 8$ V, $d_{min} = 1.3$, $\alpha_d = 1.65$) (a) source currents (b) frequency (c) source voltages (d) injected reactive power of the sources.
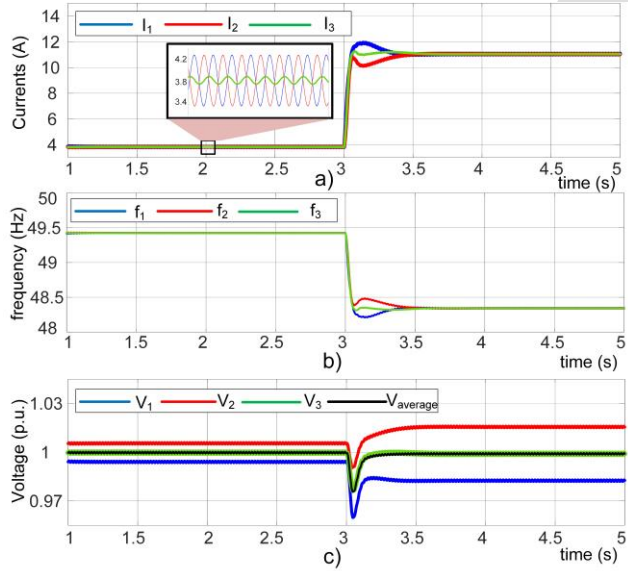

Fig. 14. Simulation results for the proposed AVCG with three power sources ($m_1 = m_2 = m_3 = 0.15$, $A = 8$ V, $d_{min} = 1.3$, $\alpha_d = 1.65$) (a) source currents (b) frequency (c) source voltages.
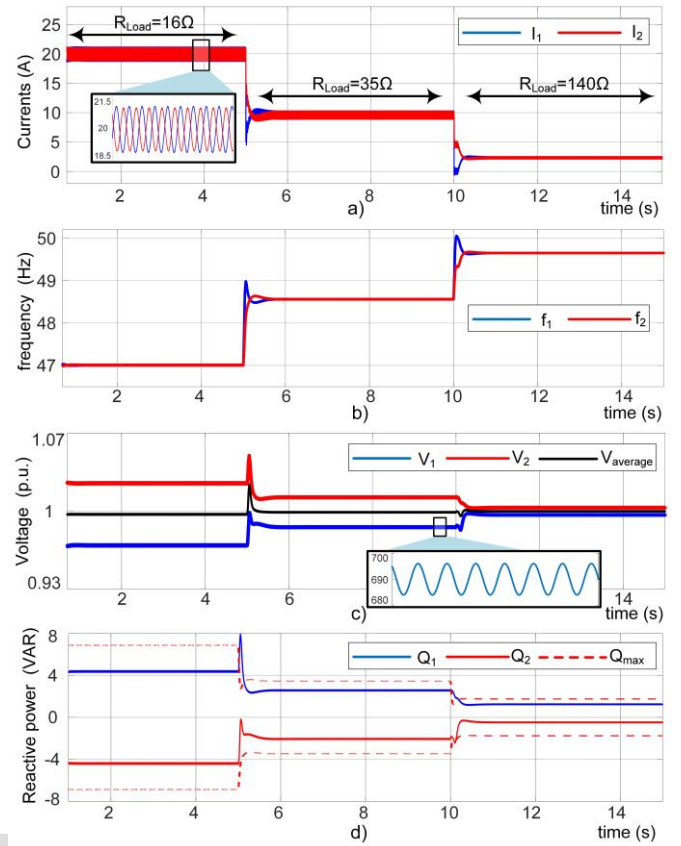

Fig. 15. Simulation results for the proposed AAIV ($m_1 = m_2 = 0.15$, $d_1 = d_2 = 5$, $A_{min} = 4$ V, $\alpha_A = 1.7$ V/Hz) (a) source currents (b) frequency (c) bus voltages (d) injected reactive power of the sources.
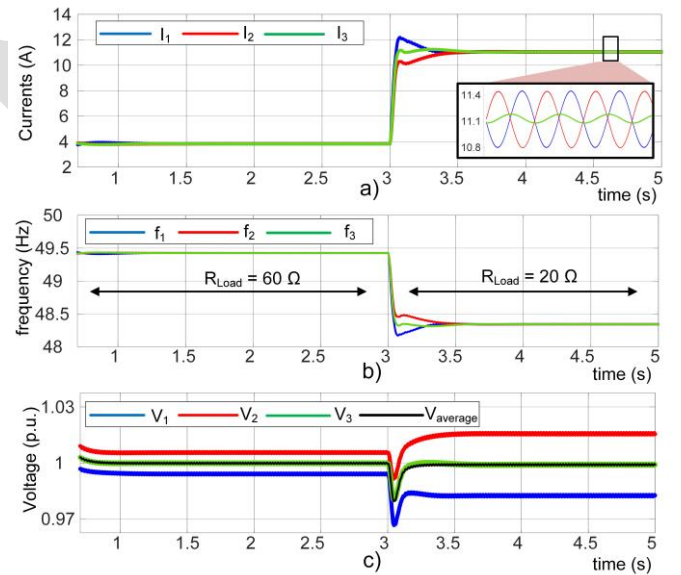
Fig. 16. Simulation results for the proposed AAIV with three power sources ($m_1 = m_2 = m_3 = 0.15$, $d_1 = d_2 = 5$, $A_{min} = 4$ V, $\alpha_A = 1.7$ V/Hz) (a) source currents (b) frequency (c) bus voltages.

Fig. 13(d). As shown in this figure, using the proposed AVCG scheme, the transferred reactive power stays in an acceptable range.

For further validation of the proposed AVCG scheme, another power source with a line resistance of 3 Ω is connected to PCC, and the new system is simulated under low and high

loadings. Parameters of the third source are like the other two sources. Results are provided in Fig. 16. At low load i.e. R_{Load} = 60 Ω, the system is stable and all the frequencies of the three sources are synchronized, and the load is equally supplied by the sources. As depicted in Fig. 14, the load is increased to 34A

at t = 2.5 Sec. As shown in Fig. 14(b), the frequencies of the injected AC voltages synchronize to a new value, and system is stable at high loading of the system. The profile of the DC voltages and the average voltage of the buses are depicted in Fig. 14(c). As shown in this figure, the average voltage of the voltage controlled buses is equal to the system reference voltage which attests the desirable voltage regulation of the system using the proposed AVCG scheme.

C. Case III: proposed AAIV scheme

The performance of the proposed AAIV is investigated through the simulation results for the system in Fig. 2. As shown in Fig. 15(a), the load is equally supplied by the two sources at different load levels, and the power-sharing accuracy is desirable. The sources injected frequencies are shown in Fig. 15(b). As shown in this figure, the injected frequencies converge to a constant value, which shows the system stability. The DC voltage of the sources are depicted in Fig. 15(c). Due to the equality of the voltage coupling gains, the average voltage of the sources is equal to the MG reference voltage, and the system voltage regulation is acceptable. The maximum transferrable reactive power and the profile of the transferred reactive power for the system using the proposed AAIV is depicted in Fig. 15(d). As shown in this figure, the maximum trnasferrable reactive power is adapted regarding the loading of the system in a way to ensure the propper performance of the system.

The performance of the proposed AAIV is further validated by connecting another power source with the line resistance of 3 Ω to PCC of the system in Fig. 2. The system performance is simulated at high and low loadings and the results are presented in Fig. 16. Fig. 16(a) shows the sources currents which shows that the sources equally supply the load current at different loadings of the system. As depicted in Fig. 16(b), the frequency of the injected AC voltage of the three sources are synchronized at both high and low loadings of the system which shows the system desirable and stable performance. The profile of the source DC voltages and their average value is depicted in Fig. 16(d). As shown in this figure, the average value of the source voltages is equal to the system reference voltage which attests the desirable voltage regulation of the system.

VII. EXPERIMENTAL RESULTS

In order to validate the proposed adaptive control strategies, a laboratory prototype is implemented. The utilized prototype contains two boost convertors controlled by their digital signal processors (DSP) as shown in Fig. 17. The two convertors are connected to the load through the line resistances. Parameters of the applied microgrid and its control systems are summarized in Table II. The test results for the two proposed methods (AVCG and AAIV) are provided and compared with those the SFDM in the following.

A. Case1: SFDM

In this case, the performance of the SFDM is validated. For the system shown in Fig. 17 with the parameters given in Table II, the test results are presented in Fig. 18(a). The load is

TABLE II
PARAMETERS OF THE IMPLEMENTED PROTOTYPE AND ITS CONTROL SYSTEM

|	Symbols	Parameter	Case1	Case2	Case3
Microgrid parameters	r_1 , r_2	line resistances	2.1 , 5 Ω		
	V_{ref}	reference voltage	205 V		
	f	reference frequency of injected AC voltage	50 Hz		
Boost convertors parameters	L_{dc}	DC inductor	1.8 mH		
	C_{dc}	DC capacitor	560 μF		
	f_{sw}	switching frequency	20 kHz		
	V_{in}	Input voltage	160 V		
	$k_{pv}+k_{iv}/S$	Voltage controller	0.2 + 0.3/S		
	$k_{pi}+k_{ii}/S$	Current controller	0.0001 + 0.001/S		
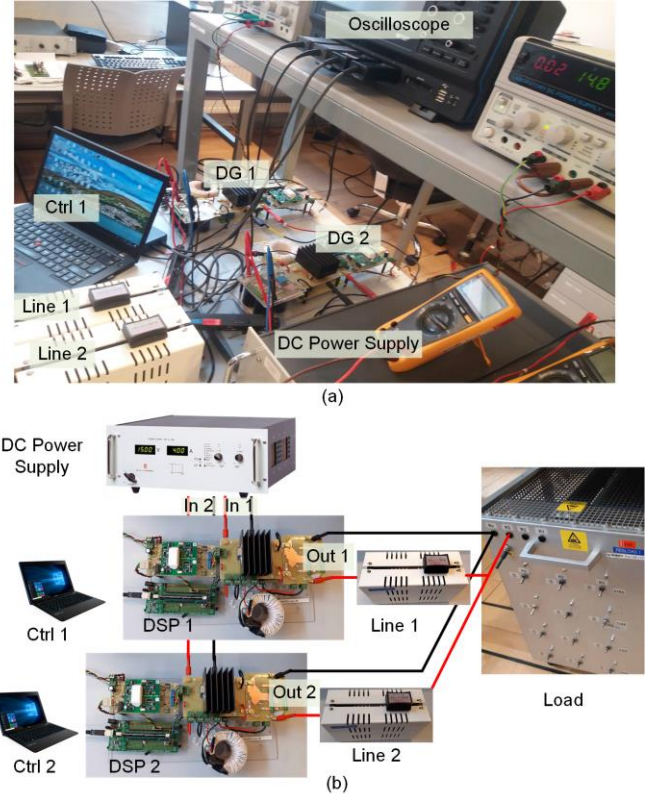
Fig. 17. Implemented test setup; (a) photograph of the applied prototype, (b) schematic of the test system with two boost converters.

increased from 3 A to 7.6 A during the test. As shown in Fig. 18, the system performance and current sharing accuracy is not desirable as the load increases.

B. Case2: AVCG scheme

The performance of the proposed AVCG scheme is verified in this case. Fig. 18(b) shows the stable operation of the system for two load levels. Furthermore, the performance of the proposed AVCG scheme is tested for different load currents as shown in Fig. 19. Based on this figure, the system is stable at all load levels and the system current sharing accuracy and performance are desirable. Therefore, as compared to the conventional method, the proposed AVCG scheme guarantees the system stable performance at all load levels.
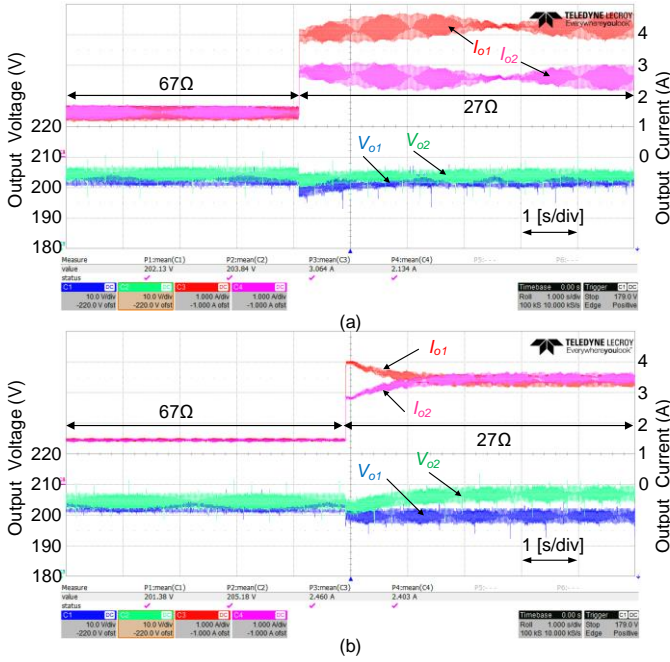
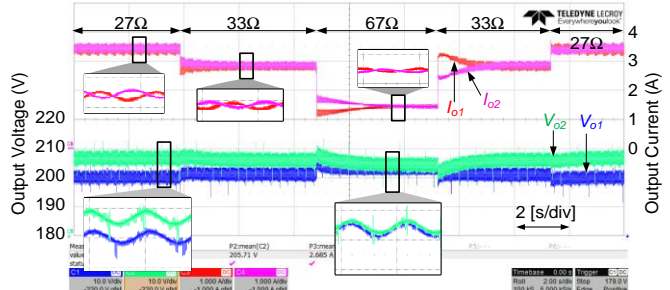Fig. 18. Experimental results for (a) SFDM (b) AVCG scheme.

Fig. 19. Experimental results for the performance of hte proposed AVCG scheme at different load levels.
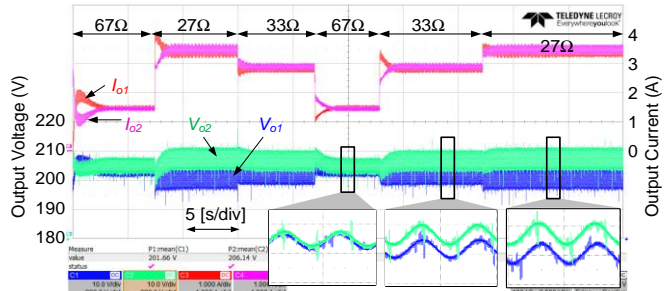

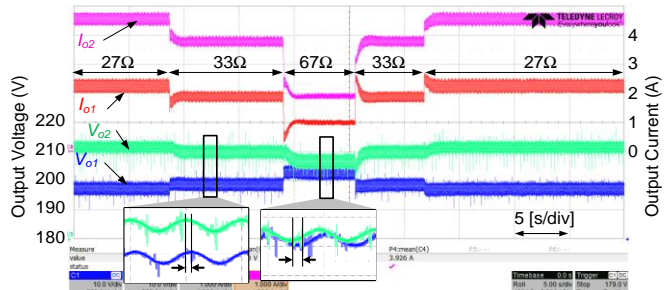Fig. 20. Experimental results for the proposed AAIV scheme under equal convertor ratings.

Fig. 21. Experimental results for the proposed AAIV scheme under unequal convertor ratings.

C. Case3: AAIV scheme

The test results for the system using the proposed AAIV is provided in Fig. 20. The load is changed several times during the test. As shown in Fig. 18, the system is stable at all load levels, and the load is equally supplied by the two sources. Therefore, as compared to the conventional method, the system stability in terms of load variations is ensured using the proposed AAIV scheme.

The effectiveness of the proposed AAIV scheme is further investigated under unequal convertor ratings ($m_1 = 0.3$, $m_2 = 0.15$) through the tests and the results are provided in Fig. 21. As shown in this figure, the system is stable at all load levels and its performance is acceptable. Also, the load current is shared among the two sources proportional to their ratings at different system loadings.

VIII. CONCLUSIONS

This paper has proposed two new approaches to enhance the performance of the SFDM for the control of DC-MGs. Considering the limited transferable reactive power in the SFDM, only can a limited range of the loads be supplied by the system. Furthermore, the SFDM suffers from some levels of instability and voltage quality issues. Using the two proposed methods, the system maximum loading is increased, and the system stability is ensured. Furthermore, the system voltage quality is enhanced. In the proposed AVCG, an adaptive coupling gain is used, and the equivalent coupling gains are regulated regarding the overall load of the MG. This keeps the transferred reactive power within the acceptable area, and makes it possible to supply higher loads with a lower amplitude of the injected AC voltage. Therefore, this method enhances the system voltage quality. In the AAIV, the amplitude of the injected AC voltage is regulated according to the MG loading condition. This enhances the system voltage quality and loading condition. The proposed schemes locally control the sources and do not require any communication infrastructure. The performance of the proposed methods has been tested by different simulations and further validated by experiments.

REFERENCES

[1] D. Boroyevich, I. Cvetkovic, R. Burgos, and D. Dong, "Intergrid: A Future Electronic Energy Network?," *IEEE J. Emerg. Sel. Top. Power Electron.*, vol. 1, no. 3, pp. 127–138, 2013.

[2] S. Peyghami, P. Davari, H. Mokhtari and F. Blaabjerg, "Decentralized Droop Control in DC Microgrids Based on a Frequency Injection Approach," *IEEE Trans. Smart Grid*, doi: 10.1109/TSG.2019.2911213.

[3] S. Peyghami, P. Davari, H. Mokhtari, P. C. Loh and F. Blaabjerg, "Synchronverter-Enabled DC Power Sharing Approach for LVDC Microgrids," *IEEE Trans. Power Electron.*, vol. 32, no. 10, pp. 8089-8099, Oct. 2017.

[4] J. Schonbergerschonberger, R. Duke and S. D. Round, "DC-Bus Signaling: A Distributed Control Strategy for a Hybrid Renewable Nanogrid," *IEEE Trans. Industrial Electronics*, vol. 53, no. 5, pp. 1453-1460, Oct. 2006.

[5] K. Sun, L. Zhang, Y. Xing and J. M. Guerrero, "A Distributed Control Strategy Based on DC Bus Signaling for Modular Photovoltaic Generation Systems With Battery Energy Storage," *IEEE Trans. Power Electron.*, vol. 26, no. 10, pp. 3032-3045, Oct. 2011.

[6] D. Chen, L. Xu and L. Yao, "DC Voltage Variation Based Autonomous Control of DC Microgrids," *IEEE Trans. Power Deliv.*, vol. 28, no. 2, pp. 637-648, April 2013.

[7] D. Chen and L. Xu, "Autonomous DC Voltage Control of a DC Microgrid With Multiple Slack Terminals," *IEEE Trans. Power Syst*, vol. 27, no. 4, pp. 1897-1905, Nov. 2012.

[8] A. Ingle, A. B. Shyam, S. R. Sahoo and S. Anand, "Quality-Index Based Distributed Secondary Controller for a Low-Voltage DC Microgrid," *IEEE Trans. Ind. Electron.*, vol. 65, no. 9, pp. 7004-7014, Sept. 2018.

[9] P. Wang, X. Lu, X. Yang, W. Wang and D. Xu, "An Improved Distributed Secondary Control Method for DC Microgrids With Enhanced Dynamic Current Sharing Performance," *IEEE Trans. Power Electron.*, vol. 31, no. 9, pp. 6658-6673, Sept. 2016.

[10] R. Han, M. Tucci, A. Martinelli, J. M. Guerrero and G. Ferrari-Trecate, "Stability Analysis of Primary Plug-and-Play and Secondary Leader-Based Controllers for DC Microgrid Clusters," *IEEE Trans. Power Syst.*, vol. 34, no. 3, pp. 1780-1800, May 2019.

[11] S. Anand, B. G. Fernandes and J. Guerrero, "Distributed Control to Ensure Proportional Load Sharing and Improve Voltage Regulation in Low-Voltage DC Microgrids," *IEEE Trans. Power Electron.*, vol. 28, no. 4, pp. 1900-1913, April 2013.

[12] V. Nasirian, A. Davoudi, F. L. Lewis and J. M. Guerrero, "Distributed Adaptive Droop Control for DC Distribution Systems," *IEEE Trans. Energy Conversion*, vol. 29, no. 4, pp. 944-956, Dec. 2014.

[13] S. Peyghami, P. Davari, and F. Blaabjerg, "System-Level Reliability-Oriented Power Sharing Strategy for DC Power Systems," IEEE Trans. Ind. Appl., vol. 55, no. 5, pp. 4865–4875, 2019.

[14] M. Mokhtar, M. I. Marei and A. A. El-Sattar, "An Adaptive Droop Control Scheme for DC Microgrids Integrating Sliding Mode Voltage and Current Controlled Boost Converters," *IEEE Trans. Smart Grid*, vol. 10, no. 2, pp. 1685-1693, March 2019.

[15] A. Khorsandi, M. Ashourloo and H. Mokhtari, "A Decentralized Control Method for a Low-Voltage DC Microgrid," *IEEE Trans. Energy Conv.*, vol. 29, no. 4, pp. 793-801, Dec. 2014.

[16] P. Prabhakaran, Y. Goyal and V. Agarwal, "Novel Nonlinear Droop Control Techniques to Overcome the Load Sharing and Voltage Regulation Issues in DC Microgrid," *IEEE Trans. Power Electron.*, vol. 33, no. 5, pp. 4477-4487, May 2018.

[17] X. Lu, K. Sun, J. M. Guerrero, J. C. Vasquez and L. Huang, "Double-Quadrant State-of-Charge-Based Droop Control Method for Distributed Energy Storage Systems in Autonomous DC Microgrids," *IEEE Trans. Smart Grid*, vol. 6, no. 1, pp. 147-157, Jan. 2015.

[18] S. Augustine, M. K. Mishra and N. Lakshminarasamma, "Adaptive Droop Control Strategy for Load Sharing and Circulating Current Minimization in Low-Voltage Standalone DC Microgrid," *IEEE Trans. Sustainable Energy*, vol. 6, no. 1, pp. 132-141, Jan. 2015.

[19] X. Lu, K. Sun, J. M. Guerrero, J. C. Vasquez and L. Huang, "State-of-Charge Balance Using Adaptive Droop Control for Distributed Energy Storage Systems in DC Microgrid Applications," *IEEE Trans. Industrial Electronics*, vol. 61, no. 6, pp. 2804-2815, June 2014.

[20] Y. Xia, W. Wei, M. Yu, X. Wang and Y. Peng, "Power Management for a Hybrid AC/DC Microgrid With Multiple Subgrids," *IEEE Trans. Power Electron.*, vol. 33, no. 4, pp. 3520-3533, April 2018.

[21] Y. Xia, W. Wei, Y. Peng, P. Yang and M. Yu, "Decentralized Coordination Control for Parallel Bidirectional Power Converters in a Grid-Connected DC Microgrid," *IEEE Trans. Smart Grid*, vol. 9, no. 6, pp. 6850-6861, Nov. 2018.

[22] A. Khorsandi, M. Ashourloo, H. Mokhtari and R. Iravani, "Automatic Droop Control for a Low Voltage DC Microgrid," *IET Generation, Transmission & Distribution*, vol. 10, no. 1, pp. 41-47, July 2016.

[23] A. Kirakosyan, E. F. El-Saadany, M. S. El Moursi, A. Yazdavar, and A. Al-Durra, "Communication-Free Current Sharing Control Strategy for DC Microgrids and Its Application for AC/DC Hybrid Microgrids," *IEEE Trans. Power Syst.*, no. To be published/ DOI: 10.1109/TPWRS.2019.2925779, pp. 1–13, 2019.

[24] S. Peyghami, H. Mokhtari, P. C. Loh, P. Davari and F. Blaabjerg, "Distributed Primary and Secondary Power Sharing in a Droop-Controlled LVDC Microgrid with Merged AC and DC Characteristics," *IEEE Trans. Smart Grid*, vol. 9, no. 3, pp. 2284-2294, May 2018.

[25] S. Peyghami, H. Mokhtari and F. Blaabjerg, "Decentralized Load Sharing in a Low-Voltage Direct Current Microgrid with an Adaptive Droop Approach Based on a Superimposed Frequency," *IEEE J. Emerg. Sel. Top. Power Electron.*, vol. 5, no. 3, pp. 1205-1215, Sept. 2017.

Mohammad Jafari was born in Sari, Iran on 1995. He received the B.Sc. in electrical power engineering from the Department of Electrical and Computer Engineering, Isfahan University of Technology in 2017. He received his M.Sc. in power electronics and electric machines from the Department of Electrical Engineering, Sharif University of Technology in 2019. His research interests include AC and DC microgrids, power quality, power electronic converters and their applications in power systems.

Saeed Peyghami (S'14–M'17) received the B.Sc., M.Sc., and Ph.D. degrees all in electrical power engineering, from the Department of Electrical Engineering, Sharif University of Technology, Tehran, Iran, in 2010, 2012, 2017, respectively. He was a Visiting Ph.D. Scholar with the Department of Energy Technology, Aalborg University, Denmark from 2015 to 2016, where he is currently a Postdoctoral Research Fellow. He was also a visiting researcher with intelligent electric power grids at Delft University of Technology, Delft, The Netherlands, form November 2019 to January 2020. His research interests include reliability, control and stability of power electronic based power systems, and renewable energies.

Hossein Mokhtari (M'03–SM'14) was born in Tehran, Iran, on August 19, 1966. He received the B.Sc. degree in electrical engineering from Tehran University, Tehran, in 1989. He received the M.Sc. degree in power electronics from the University of New Brunswick, Fredericton, NB, Canada, in 1994, and the Ph.D. degree in power electronics/power quality from the University of Toronto, Toronto, ON, Canada in 1999.

From 1989 to 1992, he worked in the Consulting Division of Power Systems Dispatching Projects, Electric Power Research Center Institute, Tehran. Since 2000, he has been with the Department of Electrical Engineering, Sharif University of Technology, Tehran, where he is currently a Professor. He is also a Senior Consultant to several utilities and industries.

Frede Blaabjerg (S'86–M'88–SM'97–F'03) was with ABB-Scandia, Randers, Denmark, from 1987 to 1988. From 1988 to 1992, he got the PhD degree in Electrical Engineering at Aalborg University in 1995. He became an Assistant Professor in 1992, an Associate Professor in 1996, and a Full Professor of power electronics and drives in 1998. From 2017 he became a Villum Investigator. He is honoris

causa at University Politehnica Timisoara (UPT), Romania and Tallinn Technical University (TTU) in Estonia.

His current research interests include power electronics and its applications such as in wind turbines, PV systems, reliability, harmonics and adjustable speed drives. He has published more than 600 journal papers in the fields of power electronics and its applications. He is the co-author of four monographs and editor of ten books in power electronics and its applications.

He has received 29 IEEE Prize Paper Awards, the IEEE PELS Distinguished Service Award in 2009, the EPE-PEMC Council Award in 2010, the IEEE William E. Newell Power Electronics Award 2014 and the Villum Kann Rasmussen Research Award 2014. He was the Editor-in-Chief of the IEEE TRANSACTIONS ON POWER ELECTRONICS from 2006 to 2012. He has been Distinguished Lecturer for the IEEE Power Electronics Society from 2005 to 2007 and for the IEEE Industry Applications Society from 2010 to 2011 as well as 2017 to 2018. In 2018 he is President Elect of IEEE Power Electronics Society. He serves as Vice-President of the Danish Academy of Technical Sciences. He is nominated in 2014, 2015, 2016 and 2017 by Thomson Reuters to be between the most 250 cited researchers in Engineering in the world.